## Characterizing entanglement at finite temperature: how does a "classical" paramagnet become a quantum spin liquid?

Snigdh Sabharwal,<sup>1</sup> Matthias Gohlke,<sup>1</sup> Paul Skrzypczyk,<sup>2</sup> and Nic Shannon<sup>1</sup>

<sup>1</sup>Theory of Quantum Matter Unit, Okinawa Institute of Science and Technology Graduate University, Onna-son, Okinawa 904-0412, Japan 
<sup>2</sup>H. H. Wills Physics Laboratory, University of Bristol, Tyndall Avenue, Bristol, BS8 1TL, UK.

(Dated: November 20, 2025)

Quantum spin liquids (QSL) are phases of matter which are distinguished not by the symmetries they break, but rather by the patterns of entanglement within them. Although these entanglement properties have been widely discussed for ground states, the way in which QSL form at finite temperature remains an open question. Here we introduce a method of characterizing both the depth and spatial structure of entanglement, and use this to explore how patterns of entanglement form as temperature is reduced in two widely studied models of QSL, the Kitaev honeycomb model, and the spin-1/2 Heisenberg antiferromagnet on a Kagome lattice. These results enable us to evaluate both the temperature at which spins within the high-temperature paramagnet first become entangled, and the temperature at which the system first develops the structured, multipartite entanglement characteristic of its QSL ground state.

In 1935, as part of a broader debate about the interpretation of quantum mechanics, Schrödinger introduced the term "entanglement" to describe the way in which mutually-exclusive experimental outcomes could be woven together in a single quantum mechanical state [1, 2]. Ninety years later, entanglement is no longer seen as a philosophical curiosity, but rather a technological resource [3], with quantum advantage sought in the entanglement of scores of qubits [4, 5]. In the context of condensed matter physics, the most celebrated example of entanglement arises in quantum spin liquids (QSL) [6–9], exotic magnetic phases where, at comparable temperatures, billions of spins can be entangled. The sharpest distinctions between QSL, conventional magnetically-ordered phases, and states driven by disorder, are all expected to be found in their entanglement properties [8–14], and significant results have also been found in the context of quantum codes [15–19]. None the less, little is known about how the entanglement characteristic of OSL behaves at finite temperature, or even whether it makes sense to discuss entanglement in candidate OSL materials, at the temperatures relevant to experiment.

Answering these questions, even in the context of a theoretical model, poses a serious technical challenge. The most widely-used tool to date, entanglement entropy, is well-posed only for pure states at zero temperature [20–22]. And while there are a number of experimentally-accessible "entanglement witnesses" which are applicable at finite temperature, each is limited in the type of entanglement it can bear witness to [13, 14, 23-27]. Evaluating more general measures of multipartite entanglement in mixed states, at finite temperature, involves optimization over all possible convex mixtures, and is an NP-hard problem [28, 29]. Fortunately, recent development of methods based on semi-definite programming (SDP) bring such questions into reach, making it possible to place precise, quatitative bounds on the entanglement encoded in the (reduced) density matrix for a given group of spins [30– 32]. The recent application of these methods to the ground states of models supporting QSL has confirmed their power [33], validating the long-held belief that multipartite entanglement in QSL is associated with cycles or "loops" of spins [9–11], as illustrated in Fig. 1. None the less, the fate of this

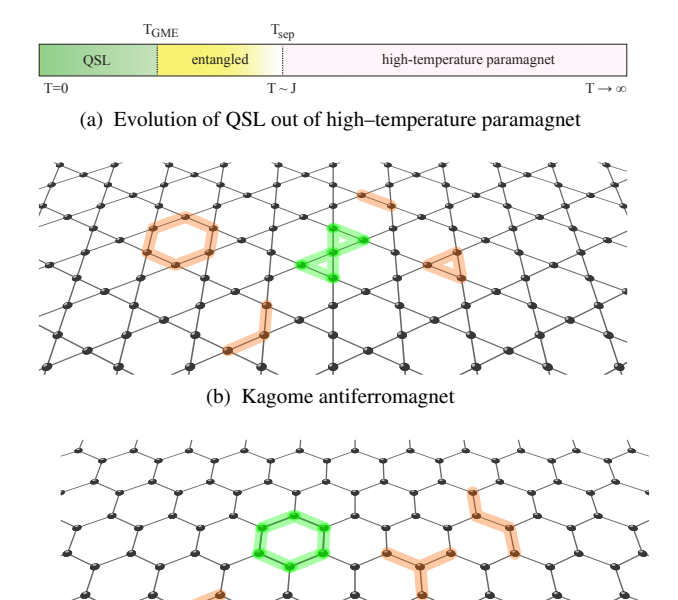


Figure 1. Evolution of a quantum spin liquid (QSL) out of a high temperature paramagnet. (a) Two–step scenario: on cooling, quantum effects enter at a temperature  $T_{\rm sep}$ , comparable with the interactions enforcing local spin correlations. Structured entanglement, characteristic of the QSL ground state, forms at a lower temperature,  $T_{\rm GME}$ . This entanglement is multipartite in nature, and confined to cycles of spins. (b) For the Kagome antiferromagnet (KAF), the shortest relevant cycle is the 6–link "bow–tie", highlighted in green. (c) For the Kitaev honeycomb model (KHM), the shortest relevant cycle is a 6–link hexagonal ring.

(c) Kitaev honeycomb model

structured entanglement at finite temperature remains an open question.

In this Letter we address the question of how the entanglement characteristic of a QSL is formed, as a frustrated spin system is cooled from a high-temperature paramagnet towards a QSL ground state. To accomplish this, we introduce a method of characterizing the *depth of entanglement* 

[34, 35] present in an arbitrary subset of spins embedded within a larger system. This is accomplished by means of the criterion of positive partial transpose (PPT) [36, 37], evaluated within an SDP. We use this approach to explore how patterns of entanglement form in clusters of spins of different geometry as a function of temperature, considering two widely-studied models of QSL: the spin-1/2 Heisenberg antiferromagnet on a Kagome lattice, and the Kitaev honeycomb model, and calculating the necessary reduced density matrices using the method of thermal pure quantum states (TPQ). In each case, we are able to confirm that multipartite entanglement at finite temperature is restricted to cycles of spins, and to identify two characteristic temperatures: the temperature at which spins within the high-temperature paramagnet first become entangled, and the temperature at which the system first develops the structured, multipartite entanglement characteristic of its QSL ground state. These results are summarised in Fig. 1

The realization that magnetic insulators could host highlyentangled phases of matter, distinct from any conventional form of magnetic order, has almost as long a history as the idea of entanglement. First explored in the context of onedimensional spin chains [38], the extension to higher dimension came through analogies with metals [39], and resonating valence bonds [40]. However the idea of a "quantum liquid" of spins didn't resonate widely until invoked to explain cuprate high-temperature superconductivity [41]. After four decades of intensive study, QSL are now firmly established as part of the landscape of condensed matter physics [6–9], with notable examples including the Kitaev honeycomb model (KHM) [42-48], sought in ruthenates and iridates [49, 50]; the spin-1/2 Heisenberg antiferromagnet on a Kagome lattice (KAF) [51–62], discussed in the context of a wide range of materials [63]; and quantum spin ice (QSI) [64-66], actively pursued in rare earth pyrochlore oxides [67–70]. None the less, because QSL are difficult to characterize, their unambiguous identification still presents many challenges, in both theory and experiment.

While conventional phases of matter are distinguished by order parameters which retain their meaning in a classical context, QSL are intrinsically quantum phases of matter, formed through the superposition of an extensive number of classical spin configurations, and capable of supporting fractionalized excitations with a topological character. By construction, such states are entangled, and the structure of the entanglement within QSL is intimately linked to the structure of their excitations and the underlying lattice. It has been widely argued that cycles play a special role in the entanglement properties of QSL [9–11]. Which of these cycles contribute to entanglement will depend on the details of the QSL under consideration.

Testing these ideas requires a tool which is capable of resolving both the spatial structure of entanglement, and of distinguishing the mutlitpartite entanglement characteristic of QSL from bipartite entanglement. And for results to have bearing on experiment, this tool must also be applicable to the mixed states found at finite temperature. Calculations of entanglement entropy can be very revealing, but are limited

to ground states [56, 58, 71]. Quantum Fisher Information (QFI) [72], which provides a bound on entanglement depth [73, 74], does not suffer from this limitation [24], and shows promise as a tool for distinguishing different quantum phases of matter through its temperature dependence [14, 75]. None the less, QFI is limited by the fact that it is tied to a particular linear operator (commonly, the lattice Fourier transform of a spin operator [24]), which must be specified in advance, and is only sensitive to a limited set of entangled states. A more universal witness is the Hamiltonian, which has been shown to provide information about the depth of entanglement at finite temperature in spin chains and some 2D frustrated spin models [35, 76, 77]. However this approach is not easily adapted to the question of determining the spatial structure of entanglement in a QSL.

Happily, while condensed-matter physicists were debating the existence of quantum spin liquids, the quantum information community were building new tools capable of characterizing entanglement in mixed states, see e.g. [23, 37, 78]. A powerful paradigm is the detection and quantification of entanglement directly from the density matrix describing a group of qubits (spins), using tools of convex optimization [32]. In particular, by relaxing separability to positive partial transposition, the problem of quantifying entanglement can be expressed as a semidefinite program, which can be efficiently solved. Moreover, by exploiting the duality of SDP's, this approach can also be used to generate entanglement witnesses which are specifically tailored to the system of interest. This overcomes the high rate of "false negatives" associated with using an "off-the-shelf" entanglement witness. The resulting witnesses have two other very desirable qualities: firstly that it retains universal validity (i.e. it can be used to detect the entanglement of other density matrices), and secondly that it provides quantitative information about entanglement for all states, by providing a lower bound on the "robustness" of that entanglement [32, 79, 80].

In the context of QSL, an important step was the publication of a recipe for quantifying multipartite entanglement, based on an SDP [30, 31]. Since this recipe applies to mixed states, it can be used to study the microscopic structure of entanglement, by applying it to reduced density matrices for clusters of spins within an extended lattice [81]. And this approach has recently been applied to the ground states of a range of models supporting QSL [33], validating the belief that multipartite entanglement is limited to cycles of spins. None the less, many questions remain open, not least the fate of the entanglement associated with these QSL ground states at finite temperature. And to answer this question it would be helpful to have a tool capable of characterizing the temperature dependence of the depth of entanglement, i.e. the minimum number of qubits which *must* be entangled for a given (mixed) state to exist. In what follows, we introduce such a tool, and use it to explore how entanglement forms in two widely studied models, the spin-1/2 Heisenberg AF on a Kagome lattice, and the Kitaev honeycomb model, as they are cooled towards their QSL ground states.

SDP for entanglement depth. We now introduce an SDP capable of placing a bound on entanglement depth [35]. The in-

put for these calculations is the reduced density matrix  $\rho_n(T)$  describing a cluster of n qubits (spins) embedded within a larger lattice, at temperature T. Our goal is to determine whether or not it is possible to write this density matrix as a probabilistic mixture (convex sum) of states involving the entanglement of no more than k-1 qubits. If  $\rho_n(T)$  fails this test, then it must be entangled to (at least) depth k.

We begin by enumerating  $\mathscr{P}_{n,k-1}$ , the set of of possible partitions  $\pi$  of n qubits to depth k-1, i.e. such that each subsystem s contains at most k-1 qubits. For example, a possible partition of n=5 qubits ABCDE, to depth k-1=2, is  $\pi=AB|CD|E$ , in which case the subsystems s are AB,CD or E. We then test whether it is possible to write the state as

$$\rho_n(T) = \sum_{\pi \in \mathscr{P}_{n,k-1}} q_{\pi} \rho_{\pi} , \ q_{\pi} \ge 0 , \sum_{\pi \in \mathscr{P}_{n,k-1}} q_{\pi} = 1 , \quad (1)$$

with the condition that

$$\rho_{\pi} = \sum_{i} p_{i}^{\pi} \bigotimes_{s \in \pi} \rho_{s}^{(i)}, \quad p_{i}^{\pi} \ge 0, \quad \sum_{i} p_{i}^{\pi} = 1, \quad (2)$$

i.e. that there is no entanglement between different subsystems s. Since enforcing the condition of strict separability, Eq. (2), is computationally challenging, we relax this to a condition of positive partial transpose, a necessary consequence of separability [32]. More precisely, we require that  $\rho_{\pi}^{T_s} \succeq 0$  for each s, where  $T_s$  denotes transposition (in a fixed, but arbitrary basis) of only the subsystem s. Any density matrix  $\rho_n(T)$  which fails the above test must be entangled to depth at least k, and will be designated "depth-k entangled".

This test can be transformed into a quantitative measure of entanglement at depth k, by determining the *robustness* of that entanglement [79, 80], i.e. how much noise must be mixed with  $\rho_n(T)$  before it can be written in the form Eq. (1). This approach leads to a *relative entropy* [82]

$$S_k[\rho_n(T)] = \ln\left(1 + \mathcal{R}_k[\rho_n(T)]\right) , \qquad (3)$$

where  $\mathcal{R}_k[\rho_n(T)]$  is a (generalized) robustness of entanglement at depth k. This can be determined through the SDP

$$1 + \mathcal{R}_{k}[\rho_{n}(T)] = \min_{\{\tilde{\rho}_{\pi}\}} \quad \text{Tr} \sum_{\pi \in \mathscr{P}_{n,k-1}} \tilde{\rho}_{\pi}$$
s.t. 
$$\sum_{\pi \in \mathscr{P}_{n,k-1}} \tilde{\rho}_{\pi} \succeq \rho_{n}(T),$$

$$\tilde{\rho}_{\pi} \succeq 0 \quad \forall \pi \in \mathscr{P}_{n,k-1},$$

$$\tilde{\rho}_{\pi}^{T_{s}} \succeq 0 \quad \forall s \in \pi, \forall \pi \in \mathscr{P}_{n,k-1},$$

where  $\tilde{\rho}_{\pi}$  are subnormalised states. (Further details of this SDP, including its relationship with optimized entanglement witnesses, are given in End Matter).

Any value of  $\mathcal{S}_k[\rho_n(T)] > 0$  signals the presence of entanglement beyond subsystems of size k-1, and thus entanglement of depth k. If we consider k=n (i.e. maximal depth),  $\mathcal{S}_{k=n}[\rho_n(T)] > 0$  implies that all subsystems are entangled, a situation more commonly known as *genuine multipartite entanglement* (GME) [30]. More generally, information about

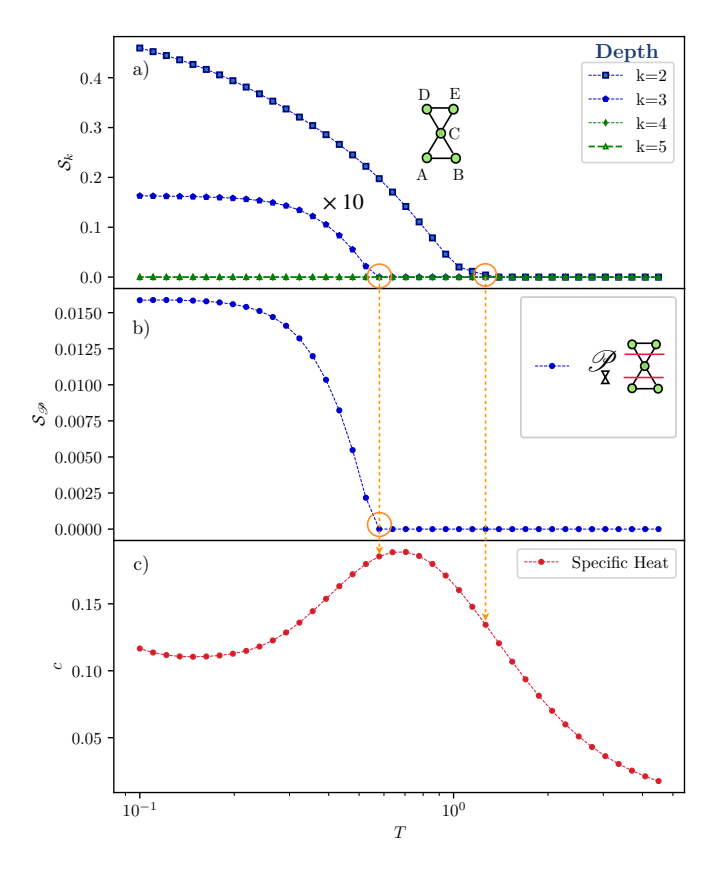


Figure 2. Evolution of entanglement as a function of temperature in the spin-1/2 Heisenberg antiferromagnet on a Kagome lattice (KAF). (a) Results for the depth of entanglement  $\mathcal{S}_k[\rho_n(T)]$  [Eq. (3)] present in the 6-link "bow-tie" cycle illustrated in Fig. 1b. Entanglement on this cycle is first detected at a temperature temperature  $T_{\bowtie}^{\text{sep}} = 1.26~J$ . Multipartite entanglement of the type needed to support a QSL is first deteched at a temperature  $T_{\text{GME}}^{\text{sep}} = 0.57~J$ . (b) Corresponding results for genuine tripartite entanglement  $\mathcal{S}_{\text{GTE}}[\rho_n(T)]$ , calculated through Eq. (5). An example of the type tripartition considered is shown in the legend. (c) Heat capacity c(T), showing how changes in entanglement correlate with changes in thermodynamic properties. Results are taken from thermal pure quantum state (TPQ) calculations for a cluster of 24 spins, as described in the end matter.

the geometrical structure of entanglement can be obtained by restricting the set of partitions considered, vis. in (4)

$$\mathscr{P}_{n,k-1} \to \mathscr{P}_{\lambda} : \mathscr{S}_{k}[\rho_{n}(T)] \to \mathscr{S}_{\lambda}[\rho_{n}(T)],$$
 (5)

where  $\mathcal{P}_{\lambda} \subset \mathcal{P}_{n,k-1}$  is a subset of partitions tailored to the question under consideration. We return to this point below, in the context of tripartite entanglement.

Finally, we note that, since we have relaxed separability to the PPT condition, our approach only detects entanglement associated with negative partial transposition. For this reason,  $\mathcal{S}_k[\rho_n(T)]$  provides a lower bound on the amount of depth-k entanglement in a system. Where required, this bound can be progressively tightened, by strengthening the PPT condition, e.g. to shareability [29], at the cost of a more complex SDP.

Results for Heisenberg antiferromagnet on a Kagome lattice. We now turn to calculations for explicit models known (or in the case of the KAF, believed) to support QSL ground states. In Fig. 2(a) we show results for the entanglement depth of the KAF as a function of temperature, evaluated on the "bow-tie" cycle shown in green in Fig. 1b. We find that density matrix on this cycle is separable for all temperatures  $T > T_{\bowtie}^{\mathsf{sep}} = 1.2 \ J$ . Because of the specific structure of this cycle, entanglement at depth k=3 acts as witness of tripartite entanglement, i.e. GME. This is detected at a temperature  $T_{\bowtie}^{\mathsf{GME}} = 0.6 J$ , just below a broad peak in heat capacity [Fig. 2(c)]. No further thresholds for depth k are detected for this cycle. We have confirmed that this measure of GME vanishes at finite temperature on all other cycles and tree-like graphs containing up to 6 spins. In contrast, bipartite entanglement at depth k=2 can be detected on a number of graphs, including the triangular cycle shown in Fig. 1b, and a decorated version of the bow-tie cycle with two additional spins (not shown).

The KAF was one of the cases considered in Ref. [33], where Lanczos diagonalization was used to calculate ground—state properties for a cluster of 36 spins. It was found that GME, studied as tripartite entanglement through a mapping onto three distinct "parties" of qubits [30], and quantified through entanglement negativity [31], was finite for the bow—tie cycle discussed above, and vanished on all other graphs of up to 6 spins. We have repeated these calculations, finding identical results at T=0, and extended the analysis to finite temperature, by adapting the SDP for entanglement depth. In Fig. 2(b) we show results for tripartite entanglement,  $\mathcal{S}_{\text{GTE}}[\rho_n(T)]$ , calculated through Eq. (5), where  $\mathcal{P}_{\text{GTE}}$  was matched to the partitions considered in [33] (see End Matter). Results are numerically identical to the GME detected by  $\mathcal{S}_{k=3}[\rho_n(T)]$  [Fig. 2(a)].

Results for Kitaev honeycomb model. We next consider how entanglement evolves at finite temperatures in KHM, focusing on the hexagonal cycle shown in Fig. 1c. In Fig. 3(a) we present results for depth of entanglement, quantified through  $\mathcal{S}_k[\rho_n(T)]$  [Eq. (3)]. We find that entanglement at depth k=2 is first detected at a temperature  $T_{\bigcirc}^{\rm sep}=0.18~J$  [Fig. 3(a)]. A cascade of bounds on depth for k=3,4,5 are found at lower temperature, with GME revealed by  $\mathcal{S}_{k=6}[\rho_n(T)]$  at  $T_{\bigcirc}^{\rm GME}=0.018~J$ .

Identifying the geometrical structure of multipartite entanglement within the KHM proves to be a more delicate question. In Fig. 3(b) we show results for the entanglement  $\mathcal{S}_{\lambda}[\rho_n(T)]$  associated with different possible partitions  $\delta\mathcal{P}_{\lambda}$ , calculated through Eq. (5) [see End Matter]. If we consider the strongest version of GME, with each spin considered separately,  $\mathcal{P}_{\lambda} = \mathcal{P}_{\bigcirc}^{(1)}$ , we recover  $T_{\bigcirc}^{\text{GME}} = 0.018~J$ , as previously found through  $\mathcal{S}_{k=6}[\rho_n(T)]$  [Fig. 3(a)]. The ground state of the KHM was another of the cases considered in [33], where a different approach was taken, with the hexagonal cycle partitioned into three equal subsystems. Following this prescription,  $\mathcal{P}_{\lambda} = \mathcal{P}_{\bigcirc}^{(3)}$ , we find  $T_{\bigcirc}^{\text{GTE}} = 0.096~J$ . However there is no unique way of dividing up the hexagon into three equal pieces, and if we include the symmetric nearestneighbour alternative on a equal footing,  $\mathcal{P}_{\lambda} = \mathcal{P}_{\bigcirc}^{(2)}$ , we find a significantly lower threshold  $T_{\bigcirc}^{(2)} = 0.025~J$ . In the absence of a physical argument linking the QSL ground state to

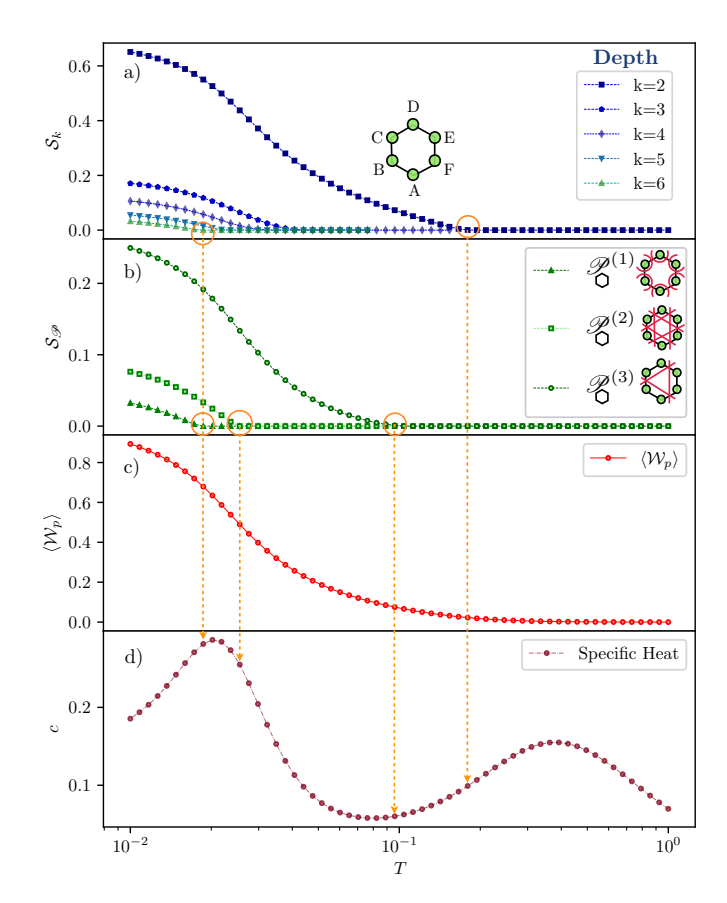


Figure 3. Evolution of entanglement as a function of temperature in the Kitaev model on a honeycomb lattice (KHM). (a) Results for the depth of entanglement,  $\mathcal{S}_k[\rho_n(T)]$  [Eq. (3)] present in the six–link hexagonal cycle illustrated in Fig. 1c. Entanglement on this cycle is first detected at a temperature  $T_{\bigcirc}^{\text{sep}}=0.18~J$ . Genuine multipartite entanglement (GME) is detected at a lower temperature  $T_{\bigcirc}^{\text{GME}}=0.018~J$ . (b) Corresponding results for the entanglement  $\mathcal{S}_{\lambda}[\rho_n(T)]$ , associated with different geometrical partitions  $\mathcal{P}_{\lambda}=\mathcal{P}_{\bigcirc}^{(m)}$  [Eq. (5), End Matter]. Tripartite entanglement is detected via  $\mathcal{P}_{\bigcirc}^{(3)}$  at a temperature  $T_{\bigcirc}^{\text{GTE}}=0.096~J$ . (c) Expectation value of plaquette operator  $\langle \mathcal{W}_p \rangle$  [Eq. (9)] associated with  $\mathbb{Z}_2$  gauge flux. (d) Heat capacity c(T) [Eq. 19], showing two–peak structure characteristic of the Kitaev spin liquid. Results are taken from thermal pure quantum state (TPQ) calculations for a cluster of 24 spins, as described in End Matter.

specifically tripartite entanglement, we make the conservative choice of associating GME with  $\mathcal{P}_{\lambda} = \mathcal{P}_{\bigcirc}^{(1)}$ , where agreement is found between  $\mathcal{S}_{\lambda}[\rho_n(T)]$  and  $\mathcal{S}_{k=n}[\rho_n(T)]$ . We have also confirmed that GME, regardless of definition, vanishes at finite temperature on all other cycles and tree–like graphs containing up to 6 spins.

General discussion of results: These results suggest a relatively simple qualitative picture of how entanglement forms as a high–temperature paramagnet is cooled towards a QSL ground state. Quantum fluctuations emerge once spins are sufficiently correlated to support them, generating entanglement, and so breaking the separability of the state at a temperarture  $T_{\text{sep}} \lesssim J$ . This change will generally be accompanied by a peak in heat capacity, coming from the entropy associ-

ated with short–range classical spin correlations (e.g, a local constraint such as the "ice rule" in quantum spin ice [65, 83–86]). At lower temperatures, quantum fluctuations act coherently, as excitations about a well defined "vacuum" (QSL ground state), giving rise to multipartite entanglement on cycles of spins for a temperature  $T_{\rm GME} \ll J$ . A second, low–temperature peak in heat capacity will typically accompany the onset of the GME, reflecting further changes in entropy coming from quantum correlations.

This simple scenario chimes with what is already known about the properties of the Kitaev honeycomb model at finite temperature, where comparison can be made with quantum Monte Carlo [45], finite-temperature Lanczos [48] and tensor-network calculations [87, 88]. These calculations provide evidence for a two-step evolution of the QSL out of the high-temperature paramagnet, with the emergence of itinerant Majorana fermions correlating with a broad peak in heat capacity at  $T \approx 0.5 J$ , and the onset of a coherent  $\mathbb{Z}_2$  flux state  $[\langle W_p \rangle \to 1]$  [Eq. (9)], being signaled by a sharper peak in heat capacity at  $T \approx 0.02 J$ . Unlike the coherent fluctuations associated with GME, the entanglement signatures of itinerant Majorana fermions in the intermediate temperature regime  $0.02~J \lesssim T \lesssim 0.5~J$  of the Kitaev model, need not be confined to closed cycles of spins. Consistent with this, we find that finite bipartite entanglement can also be detected in a decorated version of the hexagonal cycle containing 7 spins, at a slightly higher temperature  $T_{\rm sep}^{(7)} \sim 0.2~J$ . We anticipate that, were it possible to solve for entanglement on arbitrarily large graphs,  $T_{\text{sep}}$  would migrate to a temperature commensurate with upper peak in c(T). A more rigorous investigaton of this, and related finite-size effects, lies outside the scope of this manuscript, and is reserved for future work. None the less, the present calculations for  $N\,=\,24$  spins establish a clear correlation between the rise in GME and the rise in  $\langle \mathcal{W}_p \rangle$ , with the onset of the most conservative measure of GME,  $S_{k=n}[\rho_n(T)]$ , correlating well with the lower peak in

Much less is known about the finite-temperature properties of the KAF, with most studies focusing on the possibility of a QSL ground state [33, 51–62]. None the less, our results are consistent with what is known from TPQ calculations of thermodynamic properties for clusters of up to 36 spins [89, 90], over the range of temperatures considered in Fig. 3. It is also possible to obtain an independent estimate of  $T_{\rm sep}$  by comparing the energy E(T) found in TPQ calculations with the lowest energy achievable through a separable state,  $E_{\rm sep}^{\rm KAF}/N = -J/4$ , following [76, 91]. For the KAF leads to a bound  $T_{\rm sep}^{\rm E_{KAF}} = T_{\rm sep}^{\rm IM} = 1.26~J$ , identical to that found from the SDP for depth k=2 on a bowtie cycle. Applying the same technique to the KHM, where  $E_{\rm sep}^{\rm KHM}/N = -J/8$  [92], we find  $T_{\rm sep}^{\rm E_{KHM}} = 0.57~J$ . This lies a little above the upper peak in c(T), consistent with general expectations.

When it comes to experiments on quantum magnets, the main implications of these results are to provide a conceptual framework for discussing at what temperature a material becomes a QSL. The weakest criterion is  $T_{\text{sep}}$ , the temperature below which bipartite entanglement is present. This

is expected to correlate with a wide range of interesting behaviour, including the emergence of fractionalized quasiparticles, seen e.g. as a continuum in inelastic scattering. These considerations apply equally to fractionalized quasiparticles observed in proximate QSL [26, 93-96]. A much stricter criterion is  $T_{\mathsf{GME}}$ , the temperature at which entanglement starts to resemble a QSL ground state. The presence of GME, at least locally, is a necessary condition for those excitations which involve coherent fluctuations of an emergent gauge field, such as the photons of QSI [64, 65], or  $\mathbb{Z}_2$  vortices associated in the Kitaev model [42]. And from this point of view it is interesting that GME within short cycles "turns on" at a clearly-defined temperature for both of the QSL studied [Fig. 2(a,b), Fig. 3(b)], behavior reminiscent of an order parameter. No sharp anomaly is observed in c(T) at these temperatures, but broad peaks are found at similar scales. And in the case of the KHM it is the most rigorous criterion for GME,  $S_{k=n}[\rho_n(T)]$  which best matches the low–temperature peak in c(T). The presence of this peak may therefore serve as a useful proxy for GME.

Conclusions and outlook: Quantum spin liquids are quantum phases of matter distinguished by the patterns written in their entanglement. The patterns of entanglment found in QSL ground states are increasingly well understood, but the fate of this entanglement at finite temperature remains an open question. In this Letter, we have introduced a measure of the depth of entanglement found in a general mixed state, and used it to explore the way in which entanglement forms as a system is cooled from a high-temperature paramagnet towards a OSL ground state. Considering both the Kagome lattice AF [Fig. 2], and the Kitaev honeycomb model [Fig. 3], we have established a lower bound on the temperature at which spins first become entangled, and an upper bound on the temperature at which they exhibit the genuine multipartite entanglement needed to support a coherent QSL ground state. We find that GME at finite temperature is limited to cycles of spins, as previously established for QSL ground states. These results provide a conceptual framework for understanding quantum spin liquids at finite temperature, and provide a starting point for interpreting the temperature scales over which a QSL can sensibly be discussed in experiment.

The ability to characterise entanglement, and in particular the depth of entanglement, at finite temperature, also opens a new perspective on the question of quantum—classical correspondence: indeed this Letter provides two worked examples of how classical separable states at high temperature evolve into an intrinsically quantum phase at low temperature. While it is too early to speculate about the broader generality of the results, the tools used can be applied to any problem where a density matrix can be calculated in simulation, or reconstructed from measurements made on a quantum simulator. The characterization of entanglement at finite temperature therefore looks certain to have an exciting future.

Acknowledgements:. The authors are pleased to acknowledge helpful conversations with Jiahui Bao, Robert Joynt, Yoshi Kamiya, Liuke Lyu, Sandu Popescu, and Tokuro Shimokawa. SS is grateful for the hospitality of the Uni-

versity of Bristol, where a part of this work was carried out. This work was supported by the Theory of Quantum Matter Unit, OIST, and by CIFAR (through CIFAR Azrieli Global Scholarship funds). We acknowledge the use of computa-

tional resources of the Scientific Computing section of the Research Support Division at the Okinawa Institute of Science and Technology Graduate University (OIST).

- [1] E. Schrödinger, Die gegenwärtige situation in der quantenmechanik, Naturwissenschaften 23, 807 (1935).
- [2] E. Schrödinger, Discussion of probability relations between separated systems, Mathematical Proceedings of the Cambridge Philosophical Society 31, 555 (1935).
- [3] W. K. Wootters, Quantum entanglement as a quantifiable resource, Philosophical Transactions of the Royal Society A: Mathematical, Physical and Engineering Sciences 356, 1717 (1998).
- [4] Y. Kim, A. Eddins, S. Anand, K. X. Wei, E. van den Berg, S. Rosenblatt, H. Nayfeh, Y. Wu, M. Zaletel, K. Temme, and A. Kandala, Evidence for the utility of quantum computing before fault tolerance, Nature 618, 500 (2023).
- [5] Google Quantum AI and Collaborators, Observation of constructive interference at the edge of quantum ergodicity, Nature 646, 825 (2025).
- [6] P. A. Lee, An end to the drought of quantum spin liquids, Science 321, 1306 (2008).
- [7] L. Balents, Spin liquids in frustrated magnets, Nature 464, 199 (2010).
- [8] L. Savary and L. Balents, Quantum spin liquids: a review, Reports on Progress in Physics 80, 016502 (2016).
- [9] C. Broholm, R. J. Cava, S. A. Kivelson, D. G. Nocera, M. R. Norman, and T. Senthil, Quantum spin liquids, Science 367, eaay0668 (2020).
- [10] X.-G. Wen, Quantum Field Theory of Many-Body Systems: From the Origin of Sound to an Origin of Light and Electrons (Oxford University Press, 2007).
- [11] B. Zeng, X. Chen, D.-L. Zhou, and X.-G. Wen, *Quantum Information Meets Quantum Matter* (Springer New York, 2019).
- [12] H.-Q. Wu, S.-S. Gong, and D. N. Sheng, Randomness-induced spin-liquid-like phase in the spin- $\frac{1}{2}$   $J_1 J_2$  triangular heisenberg model, Phys. Rev. B **99**, 085141 (2019).
- [13] S. Sabharwal, T. Shimokawa, and N. Shannon, Witnessing disorder in quantum magnets, Phys. Rev. Res. 7, 023271 (2025).
- [14] T. Shimokawa, S. Sabharwal, and N. Shannon, Can experimentally-accessible measures of entanglement distinguish quantum spin liquids from disorder-driven "random singlet" phases?, arXiv:2505.11874 [cond-mat.str-el].
- [15] E. Dennis, A. Kitaev, A. Landahl, and J. Preskill, Topological quantum memory, Journal of Mathematical Physics 43, 4452 (2002).
- [16] C. Castelnovo and C. Chamon, Topological order in a threedimensional toric code at finite temperature, Phys. Rev. B 78, 155120 (2008).
- [17] M. B. Hastings, Topological order at nonzero temperature, Phys. Rev. Lett. 107, 210501 (2011).
- [18] O. Hart and C. Castelnovo, Entanglement negativity and sudden death in the toric code at finite temperature, Phys. Rev. B 97, 144410 (2018).
- [19] T.-C. Lu, T. H. Hsieh, and T. Grover, Detecting topological order at finite temperature using entanglement negativity, Phys. Rev. Lett. 125, 116801 (2020).
- [20] C. H. Bennett, H. J. Bernstein, S. Popescu, and B. Schumacher, Concentrating partial entanglement by local opera-

- tions, Phys. Rev. A 53, 2046 (1996).
- [21] A. Kitaev and J. Preskill, Topological entanglement entropy, Phys. Rev. Lett. 96, 110404 (2006).
- [22] M. Levin and X.-G. Wen, Detecting topological order in a ground state wave function, Phys. Rev. Lett. 96, 110405 (2006).
- [23] O. Gühne and G. Tóth, Entanglement detection, Physics Reports 474, 1 (2009).
- [24] P. Hauke, M. Heyl, L. Tagliacozzo, and P. Zoller, Measuring multipartite entanglement through dynamic susceptibilities, Nature Physics 12, 778 (2016).
- [25] A. Scheie, P. Laurell, A. M. Samarakoon, B. Lake, S. E. Nagler, G. E. Granroth, S. Okamoto, G. Alvarez, and D. A. Tennant, Witnessing entanglement in quantum magnets using neutron scattering, Phys. Rev. B 103, 224434 (2021).
- [26] A. O. Scheie, E. A. Ghioldi, J. Xing, J. A. M. Paddison, N. E. Sherman, M. Dupont, L. D. Sanjeewa, S. Lee, A. J. Woods, D. Abernathy, D. M. Pajerowski, T. J. Williams, S.-S. Zhang, L. O. Manuel, A. E. Trumper, C. D. Pemmaraju, A. S. Sefat, D. S. Parker, T. P. Devereaux, R. Movshovich, J. E. Moore, C. D. Batista, and D. A. Tennant, Proximate spin liquid and fractionalization in the triangular antiferromagnet KYbSe2, Nature Physics 20, 74 (2024).
- [27] P. Laurell, A. Scheie, E. Dagotto, and D. A. Tennant, Witnessing entanglement and quantum correlations in condensed matter: A review, Advanced Quantum Technologies 8, 2400196.
- [28] L. Gurvits, Classical deterministic complexity of edmonds' problem and quantum entanglement, in *Proceedings of the thirty-fifth annual ACM symposium on Theory of computing* (2003) pp. 10–19.
- [29] A. C. Doherty, Entanglement and the shareability of quantum states, J. Phys. A: Math. Theor. 47, 424004 (2014).
- [30] B. Jungnitsch, T. Moroder, and O. Gühne, Taming multiparticle entanglement, Phys. Rev. Lett. 106, 190502 (2011).
- [31] M. Hofmann, T. Moroder, and O. Gühne, Analytical characterization of the genuine multiparticle negativity, J. Phys. A: Math. Theor. 47, 155301 (2014).
- [32] P. Skrzypczyk and D. Cavalcanti, *Semidefinite programming* in quantum information science (IOP Publishing, 2023).
- [33] L. Lyu, D. Chandorkar, S. Kapoor, S. Takei, E. S. Sørensen, and W. Witczak-Krempa, Multiparty entanglement loops in quantum spin liquids (2025), arXiv:2505.18124 [cond-mat.strel].
- [34] A. S. Sørensen and K. Mølmer, Entanglement and extreme spin squeezing, Phys. Rev. Lett. **86**, 4431 (2001).
- [35] O. Gühne, G. Tóth, and H. J. Briegel, Multipartite entanglement in spin chains, New Journal of Physics 7, 229 (2005).
- [36] A. Peres, Separability criterion for density matrices, Phys. Rev. Lett. **77**, 1413 (1996).
- [37] M. Horodecki, P. Horodecki, and R. Horodecki, Separability of mixed states: necessary and sufficient conditions, Physics Letters A 223, 00706 (1996).
- [38] L. Hulthén, Ark. Mat. Astro. Fys. 26A (1938).
- [39] I. Pomeranchuck, The thermal conductivity of the paramagentic dielectrics at low temepratures, J. Phys. 4 4, 357 (1941).

- [40] P. Anderson, Resonating valence bonds: A new kind of insulator?, Materials Research Bulletin **8**, 153 (1973).
- [41] P. W. Anderson, The resonating valence bond state in La<sub>2</sub>CuO<sub>4</sub> and superconductivity, Science 235, 1196 (1987).
- [42] A. Kitaev, Anyons in an exactly solved model and beyond, Annals of Physics 321, 2 (2006), January Special Issue.
- [43] G. Baskaran, S. Mandal, and R. Shankar, Exact results for spin dynamics and fractionalization in the kitaev model, Phys. Rev. Lett. 98, 247201 (2007).
- [44] J. Knolle, D. L. Kovrizhin, J. T. Chalker, and R. Moessner, Dynamics of fractionalization in quantum spin liquids, Phys. Rev. B 92, 115127 (2015).
- [45] J. Nasu, M. Udagawa, and Y. Motome, Thermal fractionalization of quantum spins in a kitaev model: Temperature-linear specific heat and coherent transport of majorana fermions, Phys. Rev. B 92, 115122 (2015).
- [46] M. Gohlke, G. Wachtel, Y. Yamaji, F. Pollmann, and Y. B. Kim, Quantum spin liquid signatures in kitaev-like frustrated magnets, Phys. Rev. B 97, 075126 (2018).
- [47] M. Hermanns, I. Kimchi, and J. Knolle, Physics of the kitaev model: Fractionalization, dynamic correlations, and material connections, Annual Review of Condensed Matter Physics 9, 17 (2018).
- [48] I. Rousochatzakis, S. Kourtis, J. Knolle, R. Moessner, and N. B. Perkins, Quantum spin liquid at finite temperature: Proximate dynamics and persistent typicality, Phys. Rev. B 100, 045117 (2019).
- [49] G. Jackeli and G. Khaliullin, Mott insulators in the strong spinorbit coupling limit: From heisenberg to a quantum compass and kitaev models, Phys. Rev. Lett. 102, 017205 (2009).
- [50] Y. Matsuda, T. Shibauchi, and H.-Y. Kee, Kitaev quantum spin liquids, arXiv:2501.05608 [cond-mat.str-el].
- [51] S. Sachdev, Kagomé and triangular-lattice heisenberg antiferromagnets: Ordering from quantum fluctuations and quantumdisordered ground states with unconfined bosonic spinons, Phys. Rev. B 45, 12377 (1992).
- [52] J. T. Chalker and J. F. G. Eastmond, Ground-state disorder in the spin-1/2 kagomé heisenberg antiferromagnet, Phys. Rev. B 46, 14201 (1992).
- [53] P. Lecheminant, B. Bernu, C. Lhuillier, L. Pierre, and P. Sindzingre, Order versus disorder in the quantum heisenberg antiferromagnet on the kagomé lattice using exact spectra analysis, Phys. Rev. B 56, 2521 (1997).
- [54] M. B. Hastings, Dirac structure, rvb, and goldstone modes in the kagomé antiferromagnet, Phys. Rev. B 63, 014413 (2000).
- [55] R. R. P. Singh and D. A. Huse, Ground state of the spin-1/2 kagome-lattice heisenberg antiferromagnet, Phys. Rev. B 76, 180407 (2007).
- [56] S. Yan, D. A. Huse, and S. R. White, Spin-liquid ground state of the s = 1/2 kagome heisenberg antiferromagnet, Science 332, 1173 (2011).
- [57] Y. Iqbal, F. Becca, and D. Poilblanc, Projected wave function study of  $F_2$  spin liquids on the kagome lattice for the spin- $\frac{1}{2}$  quantum heisenberg antiferromagnet, Phys. Rev. B **84**, 020407 (2011).
- [58] H.-C. Jiang, Z. Wang, and L. Balents, Identifying topological order by entanglement entropy, Nature Physics 8, 902 (2012).
- [59] H. J. Liao, Z. Y. Xie, J. Chen, Z. Y. Liu, H. D. Xie, R. Z. Huang, B. Normand, and T. Xiang, Gapless spin-liquid ground state in the s=1/2 kagome antiferromagnet, Phys. Rev. Lett. 118, 137202 (2017).
- [60] Y.-C. He, M. P. Zaletel, M. Oshikawa, and F. Pollmann, Signatures of dirac cones in a dmrg study of the kagome heisenberg model, Phys. Rev. X 7, 031020 (2017).

- [61] A. M. Läuchli, J. Sudan, and R. Moessner,  $s=\frac{1}{2}$  kagome heisenberg antiferromagnet revisited, Phys. Rev. B **100**, 155142 (2019).
- [62] Y.-F. Jiang and H.-C. Jiang, Nature of quantum spin liquids of the  $s=\frac{1}{2}$  heisenberg antiferromagnet on the triangular lattice: A parallel dmrg study, Phys. Rev. B **107**, L140411 (2023).
- [63] M. R. Norman, Colloquium: Herbertsmithite and the search for the quantum spin liquid, Rev. Mod. Phys. 88, 041002 (2016).
- [64] M. Hermele, M. P. A. Fisher, and L. Balents, Pyrochlore photons: The U(1) spin liquid in a  $S=\frac{1}{2}$  three-dimensional frustrated magnet, Phys. Rev. B **69**, 064404 (2004).
- [65] O. Benton, O. Sikora, and N. Shannon, Seeing the light: Experimental signatures of emergent electromagnetism in a quantum spin ice, Phys. Rev. B 86, 075154 (2012).
- [66] S. Lee, S. Onoda, and L. Balents, Generic quantum spin ice, Phys. Rev. B 86, 104412 (2012).
- [67] R. Sibille, N. Gauthier, H. Yan, M. Ciomaga Hatnean, J. Ollivier, B. Winn, U. Filges, G. Balakrishnan, M. Kenzelmann, N. Shannon, and T. Fennell, Experimental signatures of emergent quantum electrodynamics in Pr<sub>2</sub>Hf<sub>2</sub>O<sub>7</sub>, Nature Physics 14, 711 (2018).
- [68] V. Porée, H. Yan, F. Desrochers, S. Petit, E. Lhotel, M. Appel, J. Ollivier, Y. B. Kim, A. H. Nevidomskyy, and R. Sibille, Evidence for fractional matter coupled to an emergent gauge field in a quantum spin ice, Nature Physics 21, 83 (2025).
- [69] E. M. Smith, E. Lhotel, S. Petit, and B. D. Gaulin, Experimental insights into quantum spin ice physics in dipole–octupole pyrochlore magnets, Annual Review of Condensed Matter Physics 16, 387 (2025).
- [70] B. Gao, F. Desrochers, D. W. Tam, D. M. Kirschbaum, P. Steffens, A. Hiess, D. H. Nguyen, Y. Su, S.-W. Cheong, S. Paschen, Y. B. Kim, and P. Dai, Neutron scattering and thermodynamic evidence for emergent photons and fractionalization in a pyrochlore spin ice, Nature Physics 21, 1203 (2025).
- [71] H. Yao and X.-L. Qi, Entanglement entropy and entanglement spectrum of the kitaev model, Phys. Rev. Lett. 105, 080501 (2010).
- [72] S. L. Braunstein and C. M. Caves, Statistical distance and the geometry of quantum states, Phys. Rev. Lett. 72, 3439 (1994).
- [73] P. Hyllus, W. Laskowski, R. Krischek, C. Schwemmer, W. Wieczorek, H. Weinfurter, L. Pezzé, and A. Smerzi, Fisher information and multiparticle entanglement, Phys. Rev. A 85, 022321 (2012).
- [74] G. Tóth, Multipartite entanglement and high-precision metrology, Phys. Rev. A 85, 022322 (2012).
- [75] C. Zhou, Z. Zhou, F. Desrochers, Y. B. Kim, and Z. Y. Meng, Quantum fisher information as a thermal and dynamical probe in frustrated magnets: Insights from quantum spin ice (2025), arXiv:2510.14813 [cond-mat.str-el].
- [76] G. Tóth, Entanglement witnesses in spin models, Phys. Rev. A 71, 010301 (2005).
- [77] O. Gühne and G. Tóth, Energy and multipartite entanglement in multidimensional and frustrated spin models, Phys. Rev. A 73, 052319 (2006).
- [78] B. M. Terhal, Bell inequalities and the separability criterion, Physics Letters A 271, 319 (2000).
- [79] G. Vidal and R. Tarrach, Robustness of entanglement, Physical Review A 59, 141 (1999).
- [80] M. Steiner, Generalized robustness of entanglement, Physical Review A 67, 054305 (2003).
- [81] T.-T. Wang, M. Song, L. Lyu, W. Witczak-Krempa, and Z. Y. Meng, Entanglement microscopy and tomography in manybody systems, Nature Communications 16, 96 (2025).

- [82] N. Datta, Max- relative entropy of entanglement, alias log robustness (2009), arXiv:0807.2536 [quant-ph].
- [83] A. Banerjee, S. V. Isakov, K. Damle, and Y. B. Kim, Unusual liquid state of hard-core bosons on the pyrochlore lattice, Phys. Rev. Lett. 100, 047208 (2008).
- [84] N. Shannon, O. Sikora, F. Pollmann, K. Penc, and P. Fulde, Quantum ice: A quantum monte carlo study, Phys. Rev. Lett. 108, 067204 (2012).
- [85] Y. Kato and S. Onoda, Numerical evidence of quantum melting of spin ice: Quantum-to-classical crossover, Phys. Rev. Lett. 115, 077202 (2015).
- [86] C.-J. Huang, Y. Deng, Y. Wan, and Z. Y. Meng, Dynamics of topological excitations in a model quantum spin ice, Phys. Rev. Lett. 120, 167202 (2018).
- [87] H. Li, D.-W. Qu, H.-K. Zhang, Y.-Z. Jia, S.-S. Gong, Y. Qi, and W. Li, Universal thermodynamics in the kitaev fractional liquid, Phys. Rev. Res. 2, 043015 (2020).
- [88] M. Gohlke, A. Iwaki, and C. Hotta, Thermal pure matrix product state in two dimensions: Tracking thermal equilibrium from paramagnet down to the Kitaev honeycomb spin liquid state, SciPost Phys. 15, 206 (2023).
- [89] S. Sugiura and A. Shimizu, Canonical thermal pure quantum state, Phys. Rev. Lett. 111, 010401 (2013).
- [90] T. Shimokawa and H. Kawamura, Finite-temperature crossover phenomenon in the s = 1/2 antiferromagnetic heisenberg model on the kagome lattice, Journal of the Physical Society of Japan 85, 113702 (2016), https://doi.org/10.7566/JPSJ.85.113702.
- [91] M. R. Dowling, A. C. Doherty, and S. D. Bartlett, Energy as an entanglement witness for quantum many-body systems, Phys. Rev. A 70, 062113 (2004).
- [92] G. Baskaran, D. Sen, and R. Shankar, Spin-s kitaev model: Classical ground states, order from disorder, and exact correlation functions, Phys. Rev. B **78**, 115116 (2008).
- [93] B. Lake, D. A. Tennant, J.-S. Caux, T. Barthel, U. Schollwöck, S. E. Nagler, and C. D. Frost, Multispinon continua at zero and finite temperature in a near-ideal heisenberg chain, Phys. Rev. Lett. 111, 137205 (2013).
- [94] A. Banerjee, C. A. Bridges, J. Q. Yan, A. A. Aczel, L. Li, M. B. Stone, G. E. Granroth, M. D. Lumsden, Y. Yiu, J. Knolle, S. Bhattacharjee, D. L. Kovrizhin, R. Moessner, D. A. Tennant, D. G. Mandrus, and S. E. Nagler, Proximate kitaev quantum spin liquid behaviour in a honeycomb magnet, Nat. Mater. 15, 733 (2016).

- [95] Y. Yamaji, T. Suzuki, T. Yamada, S.-i. Suga, N. Kawashima, and M. Imada, Clues and criteria for designing a Kitaev spin liquid revealed by thermal and spin excitations of the honeycomb iridate Na<sub>2</sub>IrO<sub>3</sub>, Phys. Rev. B 93, 174425 (2016).
- [96] M. Gohlke, R. Verresen, R. Moessner, and F. Pollmann, Dynamics of the kitaev-heisenberg model, Phys. Rev. Lett. 119, 157203 (2017).
- [97] M. Imada and M. Takahashi, Quantum Transfer Monte Carlo Method for Finite Temperature Properties and Quantum Molecular Dynamics Method for Dynamical Correlation Functions, Journal of the Physical Society of Japan 55, 3354 (1986), https://doi.org/10.1143/JPSJ.55.3354.
- [98] A. Hams and H. De Raedt, Fast algorithm for finding the eigenvalue distribution of very large matrices, Phys. Rev. E 62, 4365 (2000).
- [99] T. Iitaka and T. Ebisuzaki, Algorithm for Linear Response Functions at Finite Temperatures: Application to ESR Spectrum of  $s=\frac{1}{2}$  Antiferromagnet Cu Benzoate, Phys. Rev. Lett. **90**, 047203 (2003).
- [100] M. Machida, T. Iitaka, and S. Miyashita, ESR intensity and the Dzyaloshinsky-Moriya interaction of the nanoscale molecular magnet V<sub>15</sub>, Phys. Rev. B 86, 224412 (2012).
- [101] H. Ikeuchi, H. De Raedt, S. Bertaina, and S. Miyashita, Computation of ESR spectra from the time evolution of the magnetization: Comparison of autocorrelation and Wiener-Khinchin-relation-based methods, Phys. Rev. B 92, 214431 (2015).
- [102] H. Endo, C. Hotta, and A. Shimizu, From linear to nonlinear responses of thermal pure quantum states, Phys. Rev. Lett. 121, 220601 (2018).
- [103] M. Kawamura, K. Yoshimi, T. Misawa, Y. Yamaji, S. Todo, and N. Kawashima, Quantum lattice model solver HΦ, Computer Physics Communications 217, 180 (2017).
- [104] K. Ido, M. Kawamura, Y. Motoyama, K. Yoshimi, Y. Yamaji, S. Todo, N. Kawashima, and T. Misawa, Update of HΦ: Newly added functions and methods in versions 2 and 3, Computer Physics Communications 298, 109093 (2024).
- [105] S. Diamond and S. Boyd, CVXPY: A Python-embedded modeling language for convex optimization, Journal of Machine Learning Research (2016).
- [106] MOSEK ApS, The MOSEK Python Fusion API manual. Version 11.0. (2025).

## END MATTER

*Models*. The first model we consider is the spin–1/2 Heisenberg antiferromagnet on a Kagome lattice (KAF)

$$\mathcal{H}_{\mathsf{KAF}} = J \sum_{\langle ij \rangle} \mathbf{S}_i \cdot \mathbf{S}_j \qquad [J > 0] ,$$
 (6)

where the sum  $\langle ij \rangle$  runs over the  $1^{st}$ -neighbour bonds of a Kagome lattice. The calculations described in the main text were carried out for a 24-site cluster with periodic boundary conditions, illustrated in Fig. 4a.

The second model we consider is the Kitaev model on honeycomb lattice (KHM) [42]

$$\mathcal{H}_{\mathsf{KHM}} = \sum_{\alpha} \sum_{\langle ij \rangle \in \{\alpha\}} J_{\alpha} S_{i}^{\alpha} S_{j}^{\alpha} , \qquad (7)$$

where the sum on  $\alpha=\{x,y,x\}$  runs over the three inequivalent  $1^{st}$ -neighbour bonds of a honeycomb lattice, and we consider the isotropic parameter set

$$J_{\alpha} \equiv J > 0 \ . \tag{8}$$

The calculations described in the main text were carried out for a 24–site cluster with periodic boundary conditions, illustrated in Fig. 4b.

In the case of the Kitaev model, it is also useful to consider the operator

$$W_p = \sigma_1^x \sigma_2^y \sigma_3^z \sigma_4^x \sigma_5^y \sigma_6^z , \qquad (9)$$

which measures the  $\mathbb{Z}_2$  gauge flux on an hexagonal plaquette of the lattice [42]. Within the Kitaev QSL, in the limit  $T \to 0$ ,  $\langle \mathcal{W}_p \rangle \to 1$ .

Primal and Dual SDPs for entanglement depth. Recall from the main text that we denote by  $\mathscr{P}_{n,k-1}$  the set of partitions (subsystems) of n qubits to depth k-1, i.e. with each subsystem containing at most k-1 qubits. We denote an element of this set as  $\pi$ , and a subsystem within  $\pi$  as s. To each partition we associate a state  $\rho_{\pi}$ , and demand that  $\rho_{\pi}^{T_s} \succeq 0$  for each s.

If  $\rho_n(T)$  can be written as a mixture  $\rho_n(T) = \sum_{\pi} q_{\pi} \rho_{\pi}$ , with  $q_{\pi}$  probabilities, (satisfying  $q_{\pi} \geq 0 \ \forall \pi$  and  $\sum_{\pi} q_{\pi} = 1$ ) then it is said to be (k-1)-producible. If  $\rho_n(T)$  cannot be decomposed this way, we say it has entanglement to (at least) depth k.

We can further make this quantitative. If a state  $\rho_n(T)$  has depth-k entanglement, we can quantify how much depth-k entanglement it has by considering the amount of "noise" we must mix with it in order for it to become (k-1)-producible. That is, we can seek to find the minimum value of r such that the mixture

$$\frac{\rho_n(T) + r\sigma}{1 + r} \tag{10}$$

is (k-1)-producible, where  $\sigma$  is an arbitrary density matrix (possible highly entangled) and the mixing parameter is written as 1/(1+r), with  $0 \le r \le \infty$ . Such a parameterisation

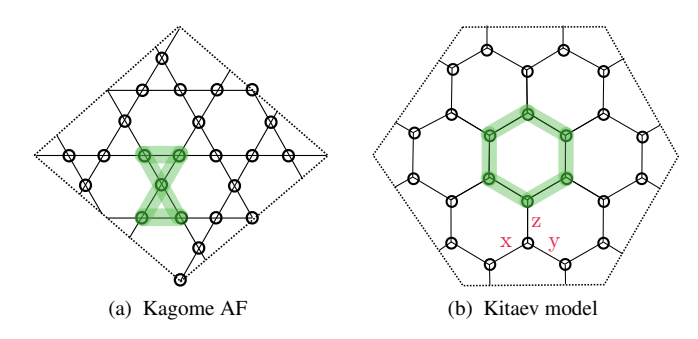


Figure 4. Clusters of the used in calculations for the Kagome lattice antiferromagnet (AF) and the Kitaev model on a honeycomb lattice. (a) 24–site cluster on Kagome lattice, showing location of 6-bond cycle used to calculate results for entanglement given in the main text. (b) 24–site cluster with full symmetry of honeycomb lattice, showing location of 6–bond cycle considered in the main text. In both cases, periodic boundary conditions are imposed, shown here through the dashed boundary of the cluster.

both allows for this to be cast as an SDP (see below), and for the optimal  $r^*$ , the quantity  $\ln(1+r^*)$  can be interpreted as a type of generalized relative entropy [82].

To turn this into an SDP, we define new variables  $\tilde{\rho}_{\pi}=(1+r)q_{\pi}\rho_{\pi}\succeq 0$  and  $\tilde{\sigma}=r\sigma\succeq 0$ , which we can view as unnormalised density matrices. In terms of these variables, (10) is (k-1)-producible if  $\rho_n(T)+\tilde{\sigma}=\sum_{\pi}\tilde{\rho}_{\pi}$ . Taking the trace of both sides of this we see that  $1+r=\mathrm{Tr}\sum_{\pi}\tilde{\rho}_{\pi}$ . We can then (i) solve for  $\tilde{\sigma}$ , i.e.  $\tilde{\sigma}=\sum_{\pi}\tilde{\rho}_{\pi}-\rho_n(T)\succeq 0$  and (ii) note that  $\rho_{\pi}^{T_s}\succeq 0$  if and only if  $\tilde{\rho}_{\pi}^{T_s}\succeq 0$  (since positive rescaling don't affect the positivity of eigenvalues of matrices). Putting everything together, minimising (1+r) is equivalent to the SDP optimization problem stated in the main text, namely

$$\min_{\{\tilde{\rho}_{\pi}\}} \quad \text{Tr} \sum_{\pi \in \mathscr{P}_{n,k-1}} \tilde{\rho}_{\pi} \tag{11}$$
s.t. 
$$\sum_{\pi \in \mathscr{P}_{n,k-1}} \tilde{\rho}_{\pi} \succeq \rho_{n}(T),$$

$$\tilde{\rho}_{\pi} \succeq 0 \quad \forall \pi \in \mathscr{P}_{n,k-1},$$

$$\tilde{\rho}_{\pi}^{T_{0}} \succeq 0 \quad \forall s \in \pi, \forall \pi \in \mathscr{P}_{n,k-1},$$

where we recall that  $A \succeq B$  is shorthand for  $A - B \succeq 0$ . This is now manifestly an SDP, with a linear objective function, and all constraints being linear inequality constraints.

Applying the duality theory of SDPs, we can obtain a second (equivalent) optimization problem, which also evaluates to  $1+\mathcal{R}_k[\rho_n(T)]$ . In particular, by introducing appropriate Lagrange multipliers for each constraint, forming a Lagrangian, and making it independent of the (primal) variables, we arrive at the following dual SDP:

$$\max_{W,\{Y_{\pi}\}} \quad \operatorname{Tr}[W\rho_{n}(T)]$$
s.t. 
$$\mathbb{1} - \sum_{s \in \pi} Y_{\pi}^{T_{s}} \succeq W \quad \forall \pi \in \mathscr{P}_{n,k-1}$$

$$W \succeq 0, \quad Y_{\pi}^{s} \succeq 0 \quad \forall s \in \pi, \forall \pi \in \mathscr{P}_{n,k-1}.$$

$$(12)$$

Eq. (12), is an optimization over quantitative entanglement witnesses for depth-k entanglement: The constraints of the dual SDP ensure that W is a quantitative witness for depth-k entanglement. The expectation value of W evaluated on any state will be non-zero only if the state has depth-k entanglement, and the value will always provide a lower bound on  $1 + \mathcal{R}_k[\rho_n(T)]$ . The SDP optimizes over all such witnesses, and is guaranteed to find a witness  $W^*$  such that  $1 + \mathcal{R}_k[\rho_n(T)] = \text{Tr}[W^*\rho_n(T)]$ .

If we consider the case of full depth, k=n, we are testing whether or not a state can be written as a mixture of states, each of which can be entangled between up to n-1 qubits (i.e. is (n-1)-producible). In this case, if (n-1) qubits can be entangled, there is only 1 remaining qubit, and hence we consider all *bipartitions* of the state. This is precisely what is considered in the context of *genuine multipartite entangle-ment* (GME), discussed below.

Geometric structure of entanglement. Entanglement depth is agnostic about the underlying geometric structure of the subsystems considered. It only takes into account the maxmium number of qubits (or particles) within a given subsystem. When considering specific physical systems, not all partitions/subsystems are equal, and hence it can be insightful also to consider specific set of partitions, and ask whether a state is 'producible' without entanglement, relative to this given set. Answering this question sheds light on the geometrical structure of the (multipartite) entanglement in the system, and can be accomplished by restricting the set of partitions considered in the SDP for entanglement depth to the reduced set  $\mathcal{P}_{\lambda}$  [Eq. (5)]. As a specific example, we consider the 6-bond cycle of the Kiteav model, and label the 6 qubits by ABCDEF in clockwise fashion, starting at an arbitrary qubit, with A and F neighbours [cf. inset to Fig. 3(b)]

A state is said to be genuine multipartite entangled (GME) if it cannot be written as a convex mixture of states which are separable with respect to any bipartition [23]. In its simplest form, GME is defined for three qubits A, B and C, and expressed in terms of the possible bipartitions of these qubits,

$$\mathscr{P}_{\mathsf{ABC}} = \{ A|BC, B|AC, C|AB \} \ . \tag{13}$$

The simplest way to generalize to a larger number of qubits is to divide these into three distinct "parties", and then to proceed by analogy with the example of three qubits. This was the approach taken in [33], where the authors considered the set

$$\mathscr{P}_{\bigcirc}^{(3)} = \{AB|CDEF, CD|ABEF, EF|ABCD\} \quad (14)$$

This can be interpreted as looking at genuine tripartite entanglement between 3 subsystems, AB, CD, EF, each comprising two qubits – a qubit and its neighbour on one side.

More generally, however, GME can be defined through any set of bipartitions which spans the qubits under considersation. Since the specifc choice  $\mathcal{P}_{\bigcirc}^{(3)}$  [Eq. (14)] breaks a symmetry of the cycle, this motivates us to consider an alternative

set of 6 partitions,

$$\mathcal{P}_{\bigcirc}^{(2)} = \{AB|CDEF, CD|ABEF, EF|ABCD, FA|BCDE, BC|DEFA, DE|FABC\}, \quad (15)$$

which restore that symmetry by pairing each qubit with both of its nearest neighbours. Testing for producibility relative to this geometrically-motivated set of partitions doesn't have an interpretation as GME, but can be viewed as a testing for a restricted type of depth-5 entanglement, where the 4 qubits must be contiguous on the hexagon.

The strongest measure of GME between six qubits is associated with the following partition

$$\mathcal{P}_{\bigcirc}^{(1)} = \{A|BCDEF, B|ACDEF, C|ABDEF, \\ D|ABCEF, E|ABCDF, F|ABCDE, \\ AB|CDEF, AC|BDEF, AD|BCEF, AE|BCDF, \\ AF|BCDE, BC|ADEF, BD|ACEF, BE|ACDF, \\ BF|ACDE, CD|ABEF, CE|ABDF, CF|ABDE, \\ DE|ABCF, DF|ABCE, EF|ABCD, \\ ABC|DEF, ABD|CEF, ABE|CDF, ABF|CDE, \\ ACD|BEF, ACE|BDF, ACF|BDE, ADE|BCF, \\ ADF|BCE, AEF|BCD\}. \quad (16)$$

Examples of partitions drawn from the sets  $\mathscr{P}_{\bigcirc}^{(1)}$ ,  $\mathscr{P}_{\bigcirc}^{(2)}$ , and  $\mathscr{P}_{\bigcirc}^{(3)}$  are shown in Fig. 3(b).

Numerical methods. The reduced density matrices  $\rho_n(T)$ , used for calculations of entanglement, were evaluated for a cluster of n spins on a graph embedded within a finite size cluster. The specific cyclic graphs used to produce the results shown in Fig. 2 and Fig. 3 of the main text are illustrated in Fig. 4. Density matrices at finite temperature were evaluated using the method of Thermal Pure Quantum states (TPQ) [89, 97–102], implemented through the package H $\Phi$  [103, 104]. At each temperature, an average

$$\rho_n(T) = \frac{1}{N_{\text{TPQ}}} \sum_{i=1}^{N_{\text{TPQ}}} \rho_n^{(i)}(T)$$
 (17)

was taken over reduced density matrices  $\rho_n^{(i)}(T)$  constructed from  $N_{\text{TPQ}}=24$  different realization a of TPQ state. We have confirmed that results for GME measures are not significantly different when evaluated for  $N_{\text{TPQ}}=50,100$ . Conventional Lanczos methods were used to evaluate reduced density matrices within the ground state,  $\rho_n(T=0)$ , for comparison with [33], and validation of finite–temeprature results.

The expectation value of the plaquette operator  $W_p$  [Eq. (9)], was evaluated as

$$\langle \mathcal{W}_p \rangle = \text{Tr}[\rho_n \mathcal{W}_p] , \qquad (18)$$

Heat capacity per spin was evaluated as

$$c(T) = \frac{\overline{\langle H^2 \rangle} - \overline{\langle H \rangle}^2}{NT^2} , \qquad (19)$$

where  $\overline{\langle \cdot \rangle}$  corresponds to the TPQ average defined in [89].

Evaluation of SDP was carried out using within the python convex optimization library CVXPY [105], using the MOSEK solver [106].